J. Cell. Mol. Med. Vol 15, No 6, 2011 pp. 1402-1414

Autophagy pathways activated in response to PDT contribute to cell resistance against ROS damage

Michael Dewaele [a], Wim Martinet [b], Noemì Rubio [a, c], Tom Verfaillie [a], Peter A. de Witte [d], Jacques Piette [c], Patrizia Agostinis [a, *]

[a] *Cell Death Research and Therapy Laboratory, Department of Molecular Cell Biology, Faculty of Medicine, Katholieke Universiteit Leuven, Leuven, Belgium*
[b] *Division of Pharmacology, University of Antwerp, Antwerp, Belgium*
[c] *GIGA-Research, Laboratory of Virology & Immunology, University of Liège, Liège, Belgium*
[d] *Laboratory for Pharmaceutical Biology, Department of Pharmaceutical Science, Faculty of Medicine, Katholieke Universiteit Leuven, Leuven, Belgium*

Received: February 26, 2010; Accepted: June 3, 2010

Abstract

Reactive oxygen species (ROS) concurrently instigate apoptosis and autophagy pathways, but the link between these processes remains unclear. Because cytotoxic ROS formation is exploited in anticancer therapy, such as in photodynamic therapy (PDT), a better understanding of the complex interplay between autophagy and apoptosis is urgently required. Previously, we reported that ROS generated by PDT with an endoplasmic reticulum (ER)-associated sensitizer leads to loss of ER-Ca^{2+} homeostasis, ER stress and apoptosis. Here we show that PDT prompted Akt-mTOR (mammalian target of rapamycin) pathway down-regulation and stimulated macroautophagy (MA) in cancer and normal cells. Overexpression of the antioxidant enzyme glutathione peroxidase-4 reversed mTOR down-regulation and blocked MA progression and apoptosis. Attenuating MA using Atg5 knockdown or 3-methyladenine, reduced clearance of oxidatively damaged proteins and increased apoptosis, thus revealing a cytoprotective role of MA in PDT. Paradoxically, genetic loss of MA improved clearance of oxidized proteins and reduced photokilling. We found that up-regulation of chaperone-mediated autophagy (CMA) in unstressed $Atg5^{-/-}$ cells compensated for MA loss and increased cellular resistance to PDT. CMA-deficient cells were significantly sensitized to photokilling but were protected against the ER stressor thapsigargin. These results disclose a stress-specific recruitment of autophagy pathways with cytoprotective function and unravel CMA as the dominant defence mechanism against PDT.

Keywords: ROS • autophagy • CMA • apoptosis • anticancer therapy • PDT

Introduction

Reactive oxygen species (ROS) are common by-products of the cellular metabolism and serve as essential signalling mediators in a variety of processes including proliferation, senescence, ageing as well as carcinogenesis [1]. However, when overproduced, ROS can directly affect cellular functions by oxidizing vital molecules that are crucial for cellular integrity, thereby causing cell demise.

Recently, ROS have also emerged as signalling mediators in macroautophagy (MA) [2–4], a major lysosomal pathway for 'in bulk' removal of entire portions of the cytoplasm, including organelles [5]. The hallmark of MA is the sequestration of the cytoplasmic material within a double membrane structure, called the autophagosome, which then fuses with the lysosome, where the cargo is degraded by the lysosomal hydrolases. Although MA can selectively remove damaged or unnecessary organelles (*e.g.* mitochondria, peroxisomes, endoplasmic reticulum [ER]), it is considered an unselective degradation process of soluble cytosolic proteins or aggregates. In contrast, chaperone-mediated autophagy (CMA) is a selective pathway for protein-by-protein removal, based on the recognition of proteins exposing a KFERQ-related targeting sequence. Recognition of this motif by the cytosolic chaperone hsc70 and its co-chaperones, targets the

*Correspondence to: P. AGOSTINIS,
Cell Death Research and Therapy Laboratory,
Department of Molecular Cell Biology, Faculty of Medicine,
Katholieke Univesiteit Leuven, Campus Gasthuisberg, O&N1,
Herestraat 49, B-3000 Leuven, Belgium.
Tel.: 00-32-16-345715
Fax: 00-32-16-345995
E-mail: patrizia.agostinis@med.kuleuven.be

doi:10.1111/j.1582-4934.2010.01118.x

chaperone-substrate complex to the lysosomal-associated membrane protein 2 (LAMP2A), the receptor for CMA, followed by translocation of the unfolded substrate in the lysosomal lumen for degradation [6, 7].

Different ROS generating molecules or signals known to promote apoptosis have recently been shown to instigate MA [2, 8–14] as well as CMA [15, 16]. Remarkably, MA function in ROS signalling appears to be highly dependent on the type of stress signal and cellular context and can be cytoprotective, favour apoptosis or instigate autophagic cell death [3, 17]. Moreover, defects in MA can also contribute to ROS generation due to the impaired removal of oxidatively damaged organelles (*i.e.* mitochondria) or proteins [3] an event that can promote carcinogenesis [18, 19].

Thus, although ROS are important bridging molecules in the cross-talk between apoptosis and autophagy pathways, the molecular mechanisms linking these processes are complex and remain poorly understood. A thorough characterization of the functional effects of autophagy pathways is particularly important when considering that cancer therapeutics devised to produce toxic amounts of ROS to eradicate tumours, might induce apoptosis concurrently with autophagy.

A well-established paradigm of anticancer therapy, killing cancer cells through oxidative stress, is photodynamic therapy (PDT) [20]. PDT utilizes a tumour-localizing photosensitizer and the local delivery of visible light to produce highly cytotoxic ROS, mainly in the form of singlet oxygen ($^1O_2$). PDT with different photosensitizers has been shown to induce both apoptotic cell death *in vitro* and *in vivo* [21, 22] and emerging studies show that PDT stimulates MA in cancer cells [23–26]. However, the exact role played by autophagy pathways in PDT is still elusive. Recently, we reported that light activation of the ER-localizing photosensitizer hypericin results in oxidative damage to the sarco(endo)plasmic Ca^{2+}-ATPase (SERCA)2 pump, which is followed by a dramatic perturbation of the ER Ca^{2+}-homeostasis, ER stress and mitochondrial apoptosis [23, 27]. Bax/Bak deficiency curtails apoptosis after PDT and triggers caspase-independent cell death utilizing aberrant MA stimulation for self-killing [23, 28].

In this study we further our understanding of the functional link between oxidative stress, autophagy pathways and cell death. We show that in cells responding to PDT, MA and CMA are stimulated and establish a direct cross-talk which is crucial to withstand ROS-induced killing. Furthermore, we show that CMA is the dominant cytoprotective pathway in PDT whereas it is dispensable for ER stress induced cell death.

Materials and methods

Reagents: Hypericin was prepared and stored as previously reported [23]. BafilomycinA1 (BafA1), 3-methyladenine (3MA), thapsigargin (TG) and doxycycline (Dox) were from Sigma-Aldrich (St. Louis, MO, USA). Hank's balanced salt solution (HBSS) starvation medium was from Invitrogen (Carlsbad, CA, USA). Anti-LC3 (microtubule-associated protein light-chain 3) antibody was from NanoTools (Teningen, Germany); anti-GFP (green fluorescent protein) from Clontech (Mountain View, CA, USA). Antibodies against phospho-p70 S6 kinase (Thr389), p70 S6 kinase, phospho-S6 ribosomal protein (Ser235/236), S6 ribosomal protein, Akt, phospho-Akt (Ser473), active caspase 3 (cleaved fragments only) and Atg5 were from Cell Signaling Technology (Danvers, MA, USA). Anti-PARP (poly(ADP-ribose) polymerase) and anti-cytochrome *c* antibodies were from BD Pharmingen (San Jose, CA USA). Anti-caspase 3 antibodies were from Calbiochem (Merck, Darmstadt, Germany). Antibodies against LAMP2A were from Zymed Laboratories (Invitrogen) and Hsc-70 from Abcam (Cambridge, UK) or AssayDesigns (Ann Arbor, MI, USA).

Cell culture and photosensitization: All cells were maintained in DMEM containing 4.5 g/l glucose and 0.11 g/l sodium pyruvate and supplemented with 2 mM glutamine, 100 units/ml penicilline, 100 μg/ml streptomycin and 10% foetal bovine serum (FBS). HeLa cells, HeLa cells overexpressing GPx4 or empty vector, AY27 and murine embryonic fibroblasts (MEFs) were incubated with hypericin for 16 hrs in FBS-containing DMEM at a concentration of 125 nM, 65 nM, 150 nM or 750 nM, respectively, to allow similar uptake and subcellular distribution of the dye. Ras^{V12} transformed MEFs and 3T3 fibroblasts were incubated with 200 nM hypericin for 2 hrs in FBS-free DMEM and 10% FBS was reconstituted after irradiation. Irradiation was performed as described before [29] at fluence rates of 2.7 J/cm^2 (HeLa, K-Ras transformed MEFs and AY27); 1.9 J/cm^2 (MEFs) and 1.5 J/cm^2 (3T3 fibroblasts).

Cell death and survival assays: Cell death was quantified with Trypan Blue Exclusion Assay and metabolic activity by the 3-[4,5-dimethylthiazol-2-yl]-2,5-diphenyl tetrazolium bromide (MTT, Sigma-Aldrich) assay as previously described [23].

Apoptosis assays: DNA fragmentation during apoptosis was measured by *ELISA^{plus}* kit (Roche Applied Science, Basel, Switzerland, following manufacturer's instructions) or by flow cytometry analysis of apoptotic SubG1 using Sytox Green (Molecular Probes, Invitrogen) as described in [30]. Phosphatidylserine exposure on the plasma membrane was measured with the 'annexinV-fluorescein isothiocyanate (FITC) apoptosis detection kit I' from BD Biosciences, according to manufacturer's instructions.

Western blotting: Preparation of cell lysates, determination of protein concentration and sample preparation for Western blotting were described in previous work [29]. Samples were processed on the Criterion^{TM} system (Bio-Rad Laboratories, Hercules, CA, USA) on a 4–12% Bis-TRIS gel and Protran 2 μm-pored nitrocellulose paper (Perkin-Elmer, Wellesley, MA, USA). Either enhanced chemiluminescence or Licor Odyssey IR imager was used as Western blot (WB) detection system. The Odyssey system was used for scanning and quantification of immunoblots.

Transmission electron microscopy (TEM): TEM was performed exactly as described in [31].

Transfection: Cells were transfected according to the manufacturer's protocol (Roche Applied Science) at a ratio of 3 μl FugeneHD: 2 μg DNA. Experiments were carried out 72 hrs after transfection to allow optimal overexpression.

siRNA transfection: Cells were transfected by adding 500 μl serum-free DMEM with 10 μl Oligofectamin (Invitrogen) and 10 μl siRNA (200 μM, Dharmacon, Thermo Fisher Scientific, Waltham, MA, USA) to 10 cm dishes with 2 ml serum-free DMEM (final concentration of 80 nM siRNA). Three hours after transfection 2.5 ml DMEM containing 10% foetal calf serum was added. Experiments were carried out 72 hrs after transfection.

Proteasome activity assay: Cells were collected and lysed in buffer A (25 mM HEPES pH 7.5, 0.3 M NaCl, 1.5 mM $MgCl_2$, 20 mM β-glycerol-phosphate, 2 mM ethylenediaminetetraacetic acid, 2 mM EGTA, 1 mM dithiothreitol, 1% (v/v) Triton X-100, 10% (v/v) glycerol). 50 μg of protein was diluted in 150 μl buffer A containing 20 μM of Suc-Leu-Leu-Val-Tyr-AMC (Bachem, Weilam Rhein, Germany). AMC release was measured

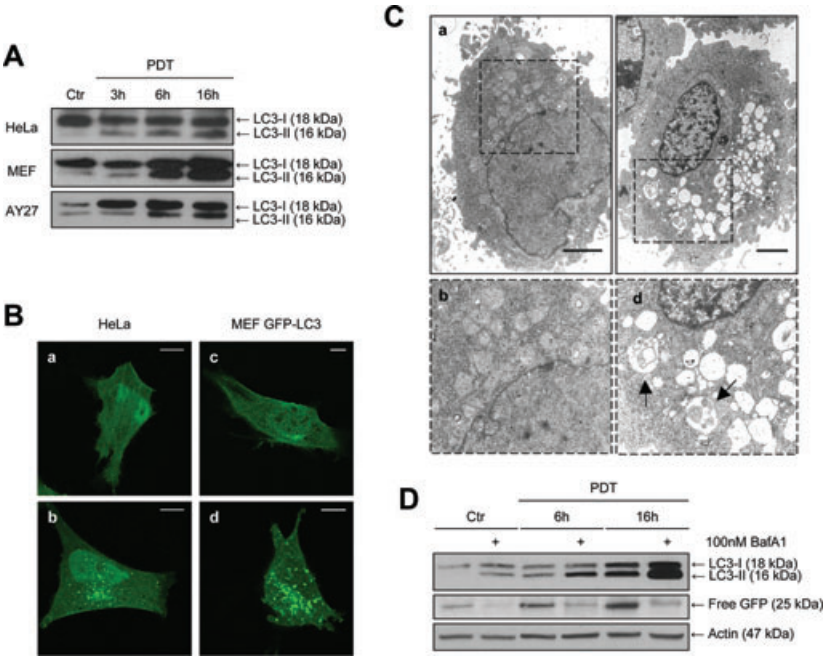

Fig. 1 Hypericin-PDT treatment evokes features of MA. All controls represent incubation with hypericin without irradiation. (**A**) Time-dependent detection of LC3-conversion by Western blot of whole cell lysates of human cervical carcinoma HeLa cells, immortalized MEFs and AY27 rat bladder carcinoma after PDT-treatment. (**B**) Confocal microscopy analysis of HeLa cells (a, b) transiently overexpressing GFP-LC3 and MEFs (c, d) stably expressing GFP-LC3. Images representative for 80% of the population of control (a, c) and cells treated 6 hrs after PDT (b, d) are shown. White scale bar in the upper right corner represents 10 μm. (**C**) Transmission electron microscopic analysis of control HeLa cells (a, b) and HeLa cells 6 hrs after PDT-treatment (c, d). EM photomicrographs representing 70% of the population are shown. (b) and (d) are magnifications of the peri-nuclear area indicated in (a) and (c). Arrows indicate vacuoles with detectable content in the treated cells (d). Black scale bar in the lower right corner represents 2 μm. (**D**) Flux analysis with MEF stably expressing GFP-LC3. HeLa cells were pre-incubated for 2 hrs with 100 nM BafA1 or vehicle (controls) before irradiation, BafA1 was present for the entire incubation period after irradiation. At the indicated time-points whole cell lysates were made for Western blot analysis.

(excitation 360 nm; emission 460 nm) for 30 min. with 2 min. intervals. Total fluorescence was plotted *versus* time and the best fitting curve was used to calculate the fluorescent units produced per minute.

OxyBlot Protein Oxidation Detection Kit was performed according to the manufacturer's protocol (Millipore, Billerica, MA, USA).

Immunocytochemistry: Cells were grown and treated on chambered coverglasses. After treatment cells were fixed with 4% p-formaldehyde (Sigma-Aldrich), permeabilized with 50% methanol (v/v in water), blocked and incubated with the primary and secondary antibodies [AlexaFluor680 and AlexaFluor488 (Invitrogen)] in blocking buffer. Background was reduced using Image-iT™ FX signal enhancer (Invitrogen). Nuclear 4′,6-diamidino-2-phenylindole (DAPI) staining was performed (1 μg/μl – Invitrogen) and cells were mounted using Prolong Gold antifade reagent (Invitrogen). Images were acquired using an Olympus FluoView FV1000 confocal microscope (Olympus, Center Valley, PA, USA) and processed with the ImageJ software. W.S. Rasbaud, ImageJ, National Institute of Health, Bethesda, MD, http://rsb.info.nih.gov/ij/.

Results

PDT induces Akt-mTOR down-regulation and stimulates functional macroautophagy in normal and transformed cells

Western blot analysis revealed that PDT-treatment of different cancer and immortalized cell lines evoked a progressive conversion of the cytosolic LC3-I into its lipidated form LC3-II, a specific biochemical marker of MA. This is as also visualized by the redistribution of GFP-tagged LC3 from a diffuse (cytosolic LC3-I) into a dotted pattern (LC3-II accumulating in autophagosomal membranes) (Fig. 1A and B). In line with these results, ultrastructural analysis of PDT-treated cells *via* TEM showed a clear vacuolization of the cytoplasm (Fig. 1C). To clarify whether accumulation of LC3-II in our paradigm reflects stimulation of the ON-rate (stimulation of autophagic degradation) of MA or results from a ROS-mediated inhibition of lysosomal function, we performed a flux-analysis using MEFs stably expressing GFP-LC3 [30]. Addition of BafA1, an inhibitor of autophagosome degradation, increased the detection of LC3-II after treatment and inhibited the release of 'free GFP', a hallmark of autophagosome degradation (Fig. 1D). This indicates that PDT stimulates MA flux.

Because induction of MA is negatively regulated by the Akt-mTOR (mammalian target of rapamycin) pathway [5], we investigated the impact of our ROS-based therapy on this core signalling pathway. Activation of p70S6K by phosphorylation on the mTOR-specific serine residue Thr389 and subsequent phosphorylation/activation of the p70S6K substrate S6 provides a valuable measure of mTOR activity [32]. As soon as 1 hr after PDT, p70S6K became progressively dephosphorylated on Thr389 and phospho-S6 levels declined subsequently (Fig. 2A). Intriguingly, S6 phosphorylation level nearly recovered to control levels 16 hrs after irradiation, suggesting the modulation of S6 phosphorylation by additional p70S6K-independent mechanisms.

Similar to p70S6K, the mTOR activator kinase Akt displayed a similar down-regulation pattern, involving a partial loss of total

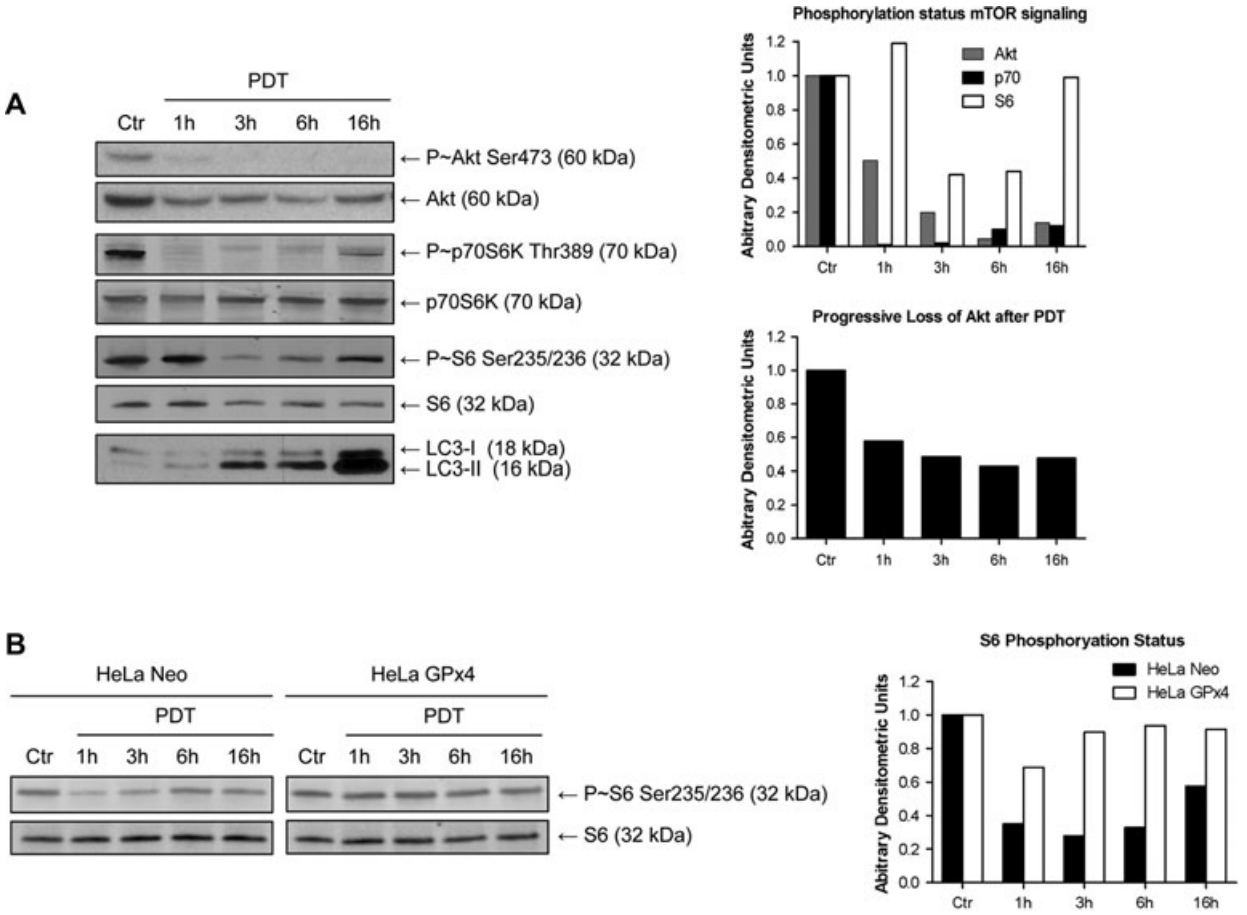

Fig. 2 Rapid inhibition of Akt-mTOR pathway after PDT. All controls represent incubation with hypericin without irradiation. (**A**) Analysis of the Akt-mTOR pathway activation-status in MEF as a function of time after PDT. *Left*: representative Western blot analysis indicating phosphorylated and total levels of Akt, p70S6Kinase and S6 ribosomal protein and LC3 conversion after PDT ($n = 3$). *Right*: Densitometric quantification of the corresponding Western blot analysis on the left. (**B**) *Left:* Representative Western blot analysis of the activation status of S6 ribosomal protein in HeLa Neo or HeLa GPx4 cells following PDT ($n = 3$). *Right:* Densitometric quantification of the corresponding Western blot analysis on the left. Arbitrary densitometric units represent phosphorylation relative to the expression level and normalized to the control condition (**A** upper graph and **B**) or expression level of Akt normalized to the expression level of control (**A** lower graph).

Akt protein, which correlated well with the kinetics of LC3-II accumulation after PDT (Fig. 2A). PDT did not affect the phosphorylation status of AMPK (data not shown), a positive regulator of MA [33], suggesting that the inhibitory effect on mTOR is mainly due to Akt down-regulation. Apart from endogenous Akt, a constitutive active form of Akt (myrAKT), overexpressed in MEF or in HeLa cells was also down-regulated after irradiation (Fig. S1). myrAKT does not require phosphatidylinositol 3-kinase signalling for its activation, thus it is unlikely that Akt down-regulation by PDT involves changes in growth factors mediated signalling. Thus, it is plausible that the down-regulation of Akt might instead involve propagation of secondary ROS from the original site of production (*i.e.* the ER) as observed in other PDT paradigms [34].

Recently, we showed that the stable overexpression of the antioxidant glutathione peroxidase 4 (GPx4) enzyme protected HeLa cells from $^1O_2$-mediated SERCA2 photo-oxidation and apoptosis after PDT [23]. Consistent with their enhanced antioxidant ability (data not shown), GPx4-expressing cells rapidly recovered phospho-S6 levels following irradiation (Fig. 2B), which correlated with a stall in LC3 conversion and a delayed onset of apoptosis (Fig. S2). These data indicate that ROS generated by PDT results in the rapid shutdown of the mTOR pathway, thereby creating an intracellular environment favouring the stimulation of MA.

Attenuation of MA enhances PDT-induced cell death

Having shown that MA is stimulated following PDT in different cells, we decided to investigate the functional role of MA on PDT-mediated cell death in apoptosis-competent cells. Although the

inhibitor of autophagosome formation 3MA [32] alone was not cytotoxic, its addition in cells exposed to PDT inhibited GFP-LC3 puncta formation (Fig. 3A), enhanced caspase 3 activation and PARP processing (Fig. 3B) and significantly increased apoptosis (Fig. 3C). An siRNA-mediated knockdown of Atg5, resulted in the reduction of the Atg5-Atg12 complex and the attenuation of MA stimulation after PDT as demonstrated by reduced LC3-conversion (Fig. 3D). Consistent with the results obtained with the inhibitor, Atg5 knockdown boosted caspase 3 cleavage and PARP processing, increased apoptotic SubG1 fraction (Fig. 3D and E) and enhanced overall photokilling (data not shown). Note that as compared to our previous studies in HeLa cells [35], the light dose used in this study was purposely milder (*i.e.* 2.7 J/cm^2) in order to measure possible pro-death inducing effects of MA inhibition.

MA is a catabolic process thought to indiscriminately remove damaged proteins, such as oxidized proteins, which are prone to aggregation, and/or organelles. Because carbonylation of amino acid side chains is a good indicator of the degree of irreversible ROS damage of proteins and carbonylated proteins are marked for degradation [36], we investigated the pattern of oxidatively damaged proteins in cells responding to PDT. PDT resulted in an initial accumulation of oxidized proteins, which progressively decreased towards control levels 16–24 hrs after irradiation, suggesting the activation of proteolytic mechanism(s) for the clearance of terminally ROS-damaged proteins. Consistent with this, reducing MA capacity by Atg5 knockdown or 3MA (data not shown) resulted in an increased accumulation of carbonylated proteins after PDT (Fig. 3F), which correlated with the sensitization towards apoptotic cell death (Fig. 3D and E). Similar results were obtained in MEFs therefore excluding a cell type-specific effect (Fig. S3A, left and middle panel).

These results show that impairing the ability of the cells to clear oxidized proteins by mitigating MA sensitizes them to ROS-mediated cell death, thus unravelling the cytoprotective role of MA in apoptosis-competent cells exposed to PDT.

MA deficiency prevents apoptosis in ROS-injured cells

To better understand the role of MA in our ROS paradigm we next evaluated the effect of MA-deficiency on PDT-induced apoptotic cell death. To this end, we used (Ras^{V12} transformed) wild-type (WT) and Atg5 knockout (KO) MEFs [37] and a Tet-Off MEF cell line [38], allowing a regulated suppression of Atg5 by Dox, to minimize effects due to clonal variation. In the latter case, complete blockage of Atg5 expression was attained after 7 days of Dox-treatment, which resulted in the complete inhibition of MA induced by PDT, starvation or tunicamycin (Fig. 4A and Fig. S3B and C).

Whereas MA attenuation by siRNA-Atg5 knockdown or 3MA increased photokilling, MA-deficiency surprisingly prevented mitochondrial cytochrome c release, caspase 3 processing, PARP cleavage and apoptosis (Fig. 4A and B) as well as overall cell death (Fig. S3A, right panel). Evaluation of phosphatidylserine exposure through annexinV-FITC labelling and cell survival within a wide range of PDT doses, confirmed that Atg5$^{-/-}$ MEFs survived better following PDT (Fig. 4C and D). Furthermore, the cytoprotective effect of MA-deficiency against photokilling was substantiated by examining the response of Ras^{V12} transformed WT and Atg5-KO MEFs after PDT (Fig. S4A and B), thus indicating that protection against ROS-induced apoptosis by MA loss occurs both in normal and transformed cells. Remarkably, along with the decreased apoptotic signalling, photosensitized Atg5$^{-/-}$ cells demonstrated an enhanced clearance of oxidized proteins as compared to their WT counterparts (Fig. 5A).

Because one of the major mechanisms for the removal of oxidatively damaged proteins in eukaryotic cells is the ubiquitin-proteasome system (UPS), we measured chymotrypsin-like UPS activity in MA-competent and MA-deficient cells exposed to PDT. Although Atg5$^{-/-}$ cells were endowed with a somewhat higher basal UPS activity, PDT reduced this proteasomal activity in both cell lines (Fig. S4C). These data suggest that the UPS cannot account for the enhanced removal of oxidized proteins in MA-deficient cells.

We next evaluated whether the reduced apoptotic response of the Atg5$^{-/-}$ cells was due to differences in ROS-mediated inactivation of the Akt-mTOR pathway. Whereas untreated Atg5$^{-/-}$ cells exhibited a somewhat higher basal level of phosphorylated/active Akt (Fig. 5B), the Akt-mTOR pathway was down-regulated equally well after PDT in MA-competent or MA-incompetent cells (Fig. 5C). A similar inhibition pattern was observed for the ERK1/2 pathway (data not shown), thus ruling out that up-regulation of growth factor and survival signalling pathways contribute to the resistance of Atg5$^{-/-}$ cells against cellular stress, as shown in a recent study [8]. Additionally, we failed to detect the calpain-mediated pro-apoptotic cleavage fragment of Atg5 [39] in ROS-damaged cells, thus excluding the possibility that resistance to photokilling by Atg5 deficiency is due to the inability to generate a pro-apoptotic Atg5 cleavage product.

Loss of MA up-regulates CMA which acts as a major defence mechanism against ROS injury

To further explain the discrepancy observed in the modulation of cellular responses to ROS by MA interference, we decided to evaluate the possibility that genetic deficiency of MA, rather than modifying its essential cytoprotective role, could stimulate the up-regulation of a compensatory mechanism with a similar protective role.

CMA has been shown to be involved in the selective removal of oxidized proteins in cells treated with H_2O_2 or the superoxide-generating drug paraquat [16]. Because activation of CMA after cellular stress is associated with a redistribution of CMA-active lysosomes from the cytosol towards the perinuclear region [16, 40], we evaluated the involvement of this lysosomal pathway by immunofluorescence microscopy. While untreated cells displayed a homogenous pattern of LAMP2A, the specific receptor for CMA, in the cytosol, PDT induced a marked redistribution of LAMP2A positive puncta to the perinuclear region of 3T3 cells (Fig. 6A) and MEFs (Fig. 6C). PDT induced also the relocalization of the CMA chaperone Hsc70 towards the perinuclear area (Fig. 6A), thus suggesting the recruitment of the CMA machinery in photosensitized

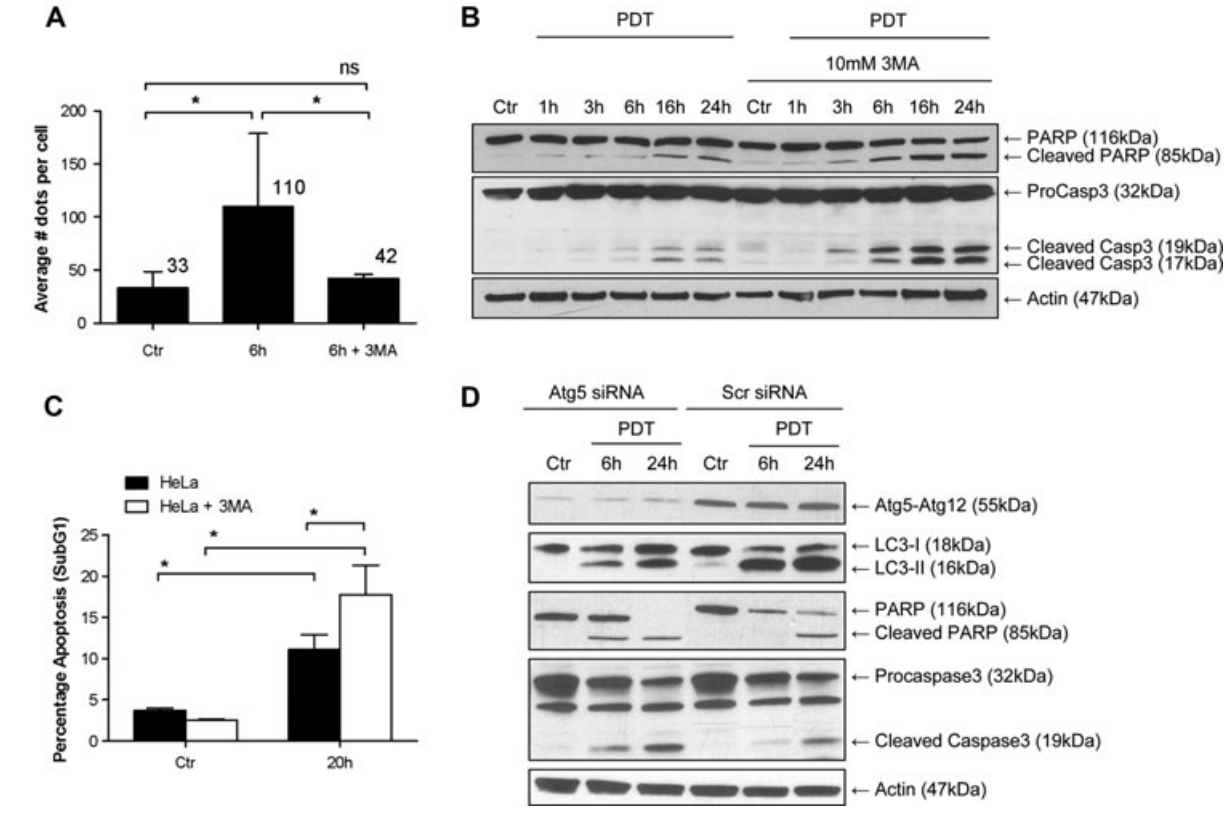

Fig. 3 Attenuation of MA enhances PDT-induced cytotoxicity. All controls represent incubation with hypericin without irradiation unless otherwise stated. (**A**) Quantification of GFP-puncta after PDT-treatment in HeLa cells transiently transfected with GFP-LC3. A subset of representative cells was analysed for their punctuated pattern in control cells and 6 hrs after treatment in the absence or presence of 10 mM 3MA. Cells were digitally processed with the ImageJ software and manually supervised. The bar values are indicated in the graph. $^*P < 0.05$ under the Student's t-test, ns: not significant. (**B**) HeLa cells were PDT-treated in the absence or presence of 10 mM 3MA and Western blot analysis of caspase 3 activation and PARP cleavage was carried out at the indicated time-points after irradiation. Representative Western blot is shown ($n = 3$). Actin was used to monitor equal loading. (**C**) Flow cytometric cell cycle analysis determining the apoptotic SubG1 fraction in PDT-treated HeLa cells in the presence or absence of 10 mM 3MA. The graph represents the mean ± S.D. of three independent experiments carried out in duplicate. $^*P < 0.05$ under the Student's t-test. 3MA was added to the cells immediately after irradiation to avoid toxicity caused by the light exposure of the inhibitor and remained in the culture medium throughout the incubation time. Controls with or without 3MA were harvested at the last evaluated time-point (**A**–**C**). (**D**) HeLa cells were transfected with Atg5 siRNA or scrambled (non-targeting) siRNA (Scr siRNA) before PDT-treatment. At the indicated time-points after PDT cell lysates were subjected to Western blot analysis with the indicated antibodies. Representative Western blot is shown ($n = 3$). Actin was used to monitor equal loading. (**E**) Apoptotic SubG1 fraction in PDT-treated HeLa cells transfected with control or Atg5 siRNA. The graph represents the mean ± S.D. of two independent experiments carried out in duplicate. $^*P < 0.05$ under the Student's t-test. (**F**) *Left:* Total cell lysates were analysed for the presence of carbonylated protein side chains with OxyBlot Protein Oxidation Detection Kit after PDT in scrambled-siRNA or Atg5-siRNA transfected HeLa cells. Actin was used as a loading control. *Right:* The graph represents the densitometric values of the OxyBlot normalized to actin and expressed as fold increase to controls. During OxyBlot procedure, hypericin was omitted from the controls to minimize effects of background irradiation during manipulation of the samples.

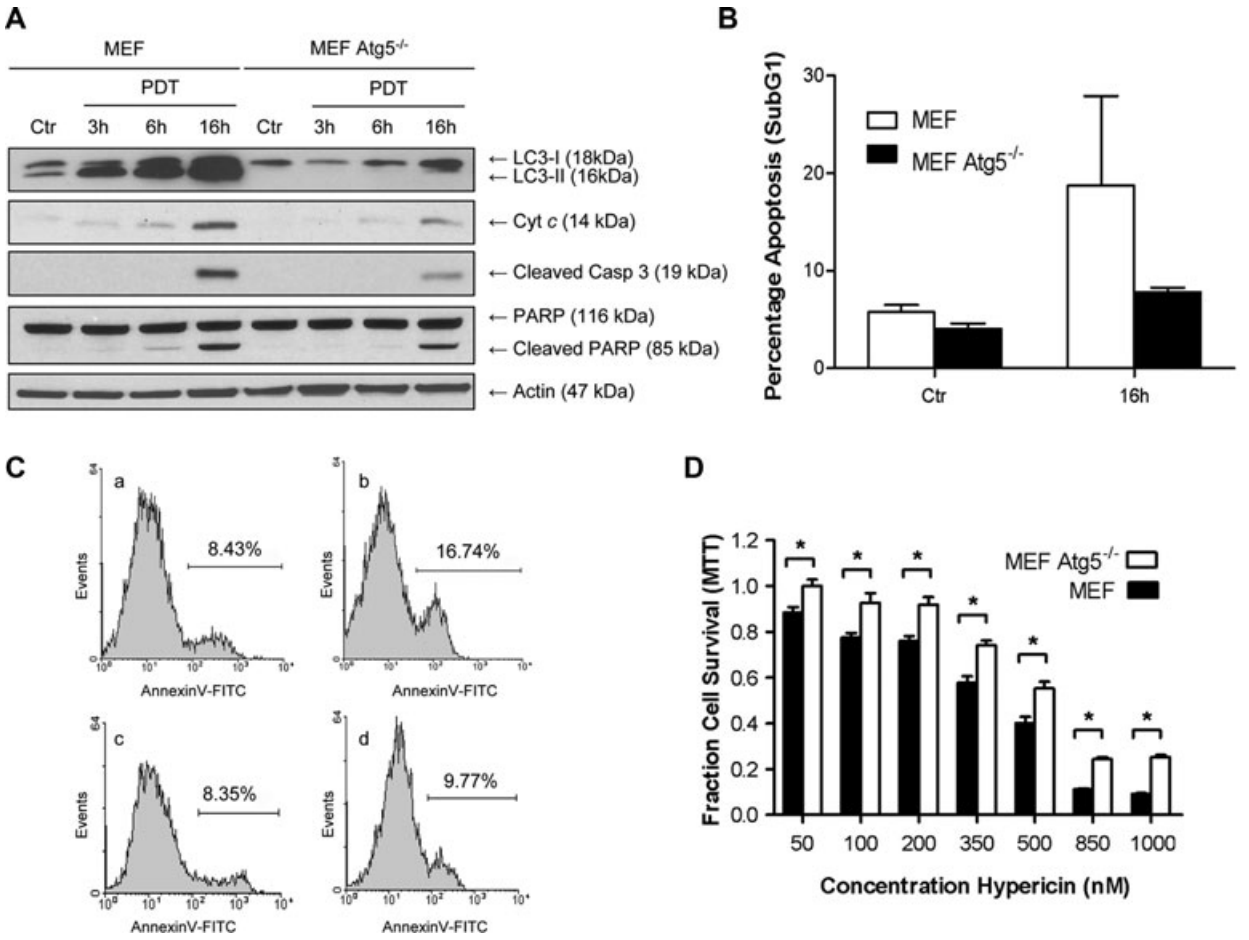

Fig. 4 Constitutive repression of MA prevents PDT-mediated cell death. All controls represent incubation with hypericin without irradiation. (**A**) Total cell lysates of MEF and Atg5$^{-/-}$ MEF were made at the indicated time-points and analysed by Western blot for LC3-conversion, caspase 3 activation and PARP cleavage. Actin was used as a loading control. A representative Western blot ($n = 3$) is shown. In a parallel experiment, subcellular fractions were made for Western blot analysis of cytochrome c release in the cytosol. (**B**) Apoptotic SubG1 fraction in PDT-treated MEF and Atg5$^{-/-}$ MEF. The graph represents the mean ± S.D. of two independent experiments. (**C**) Representative flow cytometric analysis of phosphatidylserine externalization as measured by annexinV-FITC staining in MEF (a and b) and Atg5$^{-/-}$ MEF (c and d) in control cells (a and c) and 6 hrs after PDT (b and d). The indicated percentage is the annexinV^{+} fraction. (**D**) Representative dose–response curve for PDT treatment with different concentrations of hypericin (as indicated) in MEF and Atg5$^{-/-}$ MEF as evaluated by MTT assay. The curve shows the surviving fraction of cells 16 hrs after treatment. Cell survival is expressed as the fraction surviving cells with respect to the controls. *$P < 0.05$ under the Student's t-test for a 6-fold replicate.

cells. Moreover, a fraction of the total pool of LAMP2A positive lysosomes co-localized with Hsc70, thus indicating CMA activation by PDT in MA-competent cells (Fig. 6B).

Notably, Atg5$^{-/-}$ MEFs exhibited a perinuclear distribution of CMA-competent lysosomes in unstressed conditions (Fig. 6C), consistent with the constitutive activation of CMA in MA-deficient cells reported in a recent study [40].

We then hypothesized that if up-regulation of CMA in Atg5-deficient cells was responsible for their increased resistance towards PDT and efficient clearance of oxidized proteins (Fig. 5A), LAMP2A-deficient CMA-incompetent cells [41] would be highly sensitized to PDT. Consistent with this, LAMP2A deficiency accelerated the pattern of caspase 3 activation and PARP cleavage, correlating with a persistent pattern of protein carbonylation (Fig. 7A, C and E) and resulting in a significant sensitization of these cells to PDT-induced cell death within a wide range of PDT doses (Fig. 7D). Because LAMP2A-deficient cells were extremely vulnerable to PDT, we used a milder dose (*i.e.* reduced hypericin concentration and light dose) to evaluate apoptotic parameters, which is reflected by a reduced pattern of protein carbonylation, caspase 3 processing and cell death in these fibroblasts as compared to MEFs (Fig. 7A, C–E).

Interestingly, LC3-conversion was enhanced in LAMP2A-deficient fibroblasts after PDT in comparison to their WT counterparts (Fig. 7B), in agreement with the increased MA capacity in the absence of CMA [42]. In spite of this, LAMP2A$^{-/-}$ cells showed a defective clearance of ROS-damaged proteins (Fig. 7E) as compared

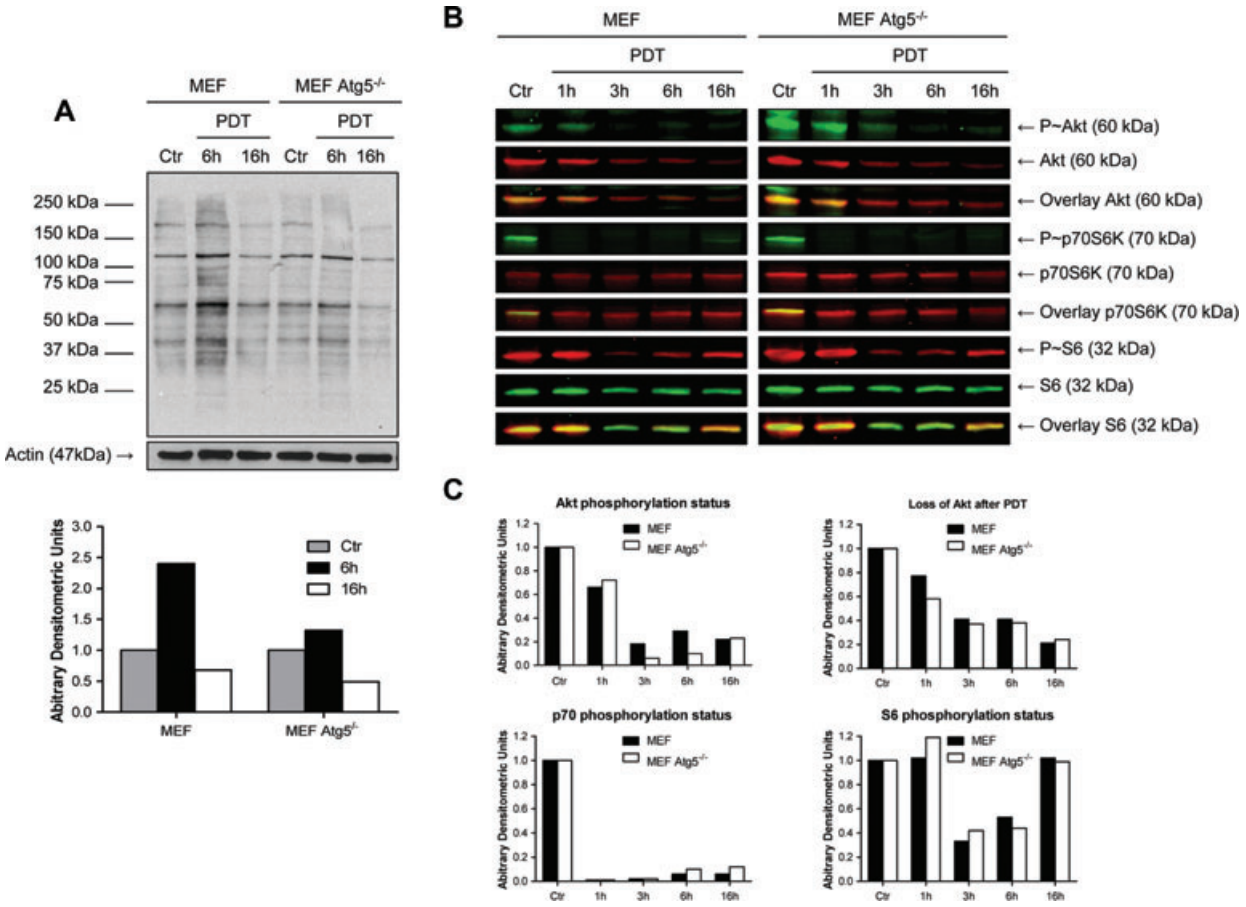

Fig. 5 MA deficiency reduces PDT-mediated oxidative damage to intracellular proteins without affecting the Akt-mTOR signalling. (**A**) *Left:* Total cell lysates were analysed for the presence of carbonylated protein side chains after PDT in MEF and Atg5$^{-/-}$ MEF, a representative OxyBlot carried out as described in Figure 3, is shown. Actin was used as a loading control ($n = 3$). *Right:* The graph represents the densitometric values of the OxyBlot normalized to actin and expressed as fold increase to controls. (**B**) Representative Western blot and densitometric analysis (**C**) of the Akt-mTOR pathway activation-status in MEF and Atg5$^{-/-}$ MEF after PDT (as shown in Fig. 2).

to their CMA-proficient counterparts, thus suggesting that impaired clearance of CMA substrates increases the cytotoxic effects of PDT.

In contrast, treatment of LAMP2A$^{-/-}$ cells with the ER-stress agent TG, which mimics the PDT-mediated blockage of the SERCA2 pumps [23] without directly altering the cellular redox-state, resulted in a significant reduction of cell death as compared to WT cells (Fig. S5A). Moreover, up-regulation of CMA in the Atg5$^{-/-}$ MEF was unable to compensate for the loss of MA function following TG (Fig. S5B). All together, these results show that CMA is the predominant cytoprotective mechanism in photosensitized and ROS-damaged cells, while TG relies exclusively on MA for cell survival.

Discussion

Although increasing evidence indicate ROS as intracellular mediators of autophagy pathways as well as cell death, the interplay between these processes remains largely unclear. In this study we show that ROS generated by PDT stimulates MA along with CMA, a lysosomal pathway of protein-by-protein degradation, whose functional contribution in cell death has not been investigated yet in the context of ROS-mediated anticancer therapies. We found that although both autophagy pathways are functionally linked and limit further propagation of ROS injury by the clearance of oxidatively damaged proteins, CMA acts as a major defensive mechanism against PDT.

Stimulation of MA by PDT correlated well with the down-regulation of Akt-mTOR-p70S6K pathway, a known permissive signal for MA, and these processes were counteracted by the antioxidant enzyme GPx4, positioning ROS production up-stream of MA induction. ROS, in the form of H_2O_2 [43] or photogenerated by the lysosomal/endosomal associated photosensitizer $AlPcS_{2a}$ [44] can directly affect mTOR, whereas Akt is a target of the SOD inhibitor 2-methoxyestradiol (2-ME) [45]. This suggests that elements of the Akt-mTOR pathway, which is crucially involved in the

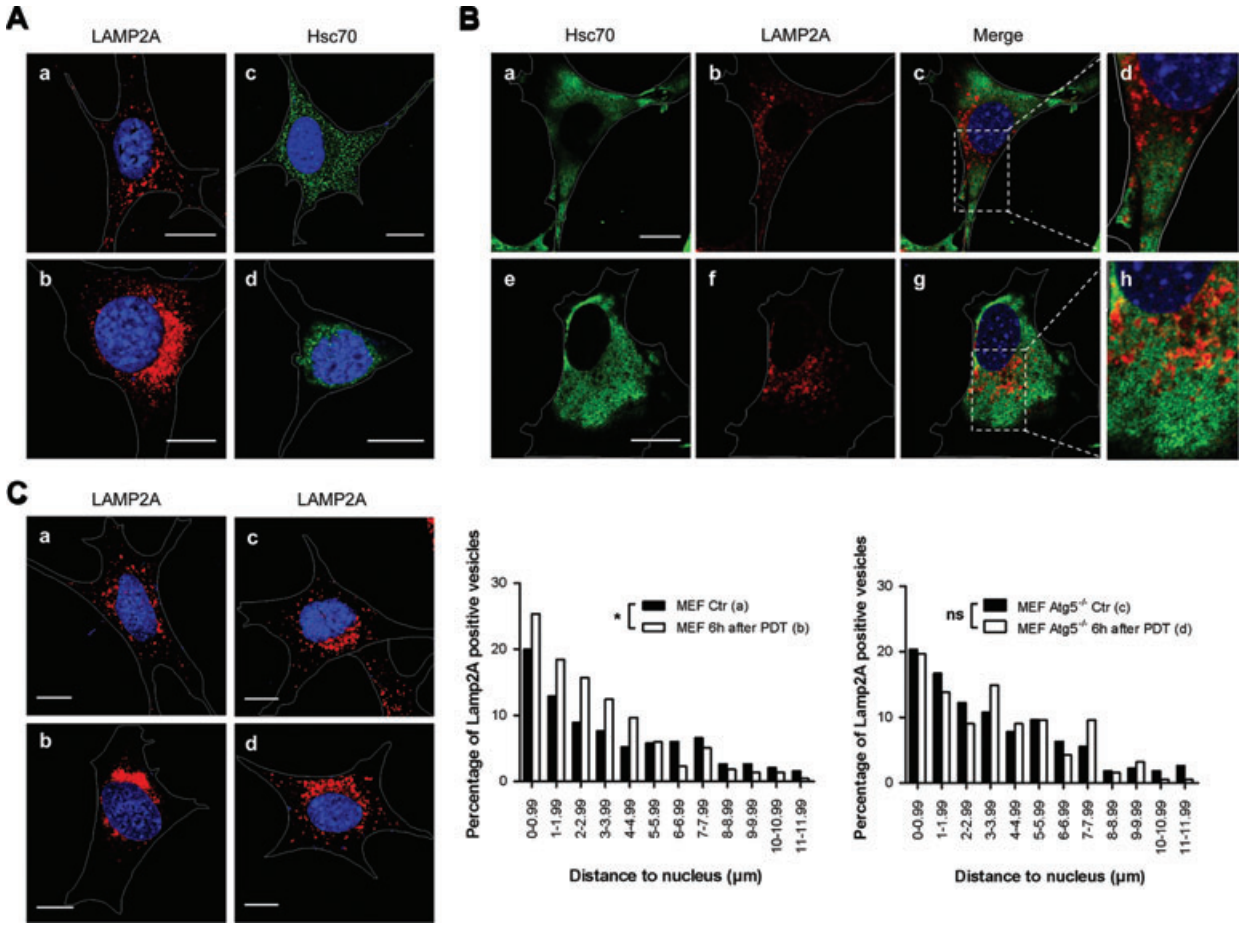

Fig. 6 CMA is up-regulated in MA-deficient cells and stimulated by PDT-treatment. All controls represent incubation with hypericin without irradiation. (**A**) Confocal analysis of LAMP2A and Hsc70 immunostaining in untreated cells (a, c) or 6 hrs after PDT-treated (b, d) in 3T3 fibroblasts. DAPI was used for nuclear counterstaining. (**B**) Confocal analysis of Hsc70 (green, a and e) and LAMP2A (red b, f) co-immunostaining in untreated (a, b) and 6 hrs after PDT-treated (e, f) MEFs. The colocalization image is shown for the control (c) and the treated cells (g). DAPI was used as a nuclear counterstain and (d) and (h) present magnifications of the areas indicated in (c) and (g), respectively. The images are representative for approximately 70% of the cellular population after PDT. (**C**) Confocal analysis of LAMP2A immunostaining in untreated cells (a, c) or 6 hrs after PDT-treated (b, d) cells. MEF (a and b), $Atg5^{-/-}$ MEF (c and d). Red fluorescence represents LAMP2A immunostaining and blue fluorescence (DAPI) was used for nuclear counterstaining. The images are representative for approximately 70% of the cellular population after PDT. The graphs represent the distribution of $LAMP2A^{+}$ vesicles respect to the nucleus. $^{*}P < 0.0001$ for the Mann-Whitney test, ns: not significant. six cells were analysed per condition using the ImageJ software. The scale bar represents 15 μm for all the images shown.

initiation phases of MA, provide a regulatory and redox-sensitive step in the ROS-mediated cascade triggering MA.

This study shows that PDT is able to stimulate MA in transformed as well as in normal immortalized cells. From a therapeutic point of view, the unselective stimulation of autophagy pathways in both normal and cancer cells by PDT is likely not relevant, because the selective action of this anticancer treatment relies on local delivery of the activating light, thus sparing the normal surrounding tissue [20, 21].

Importantly, reducing MA capacity by 3-MA or by silencing Atg5 expression sensitized cells to apoptotic cell death, thus revealing the intrinsic pro-survival role of this degradation mechanism in PDT. Unlike PDT, other promising ROS-inducing cancer therapeutics, such as 2-ME [9] or selenite [11] failed to induce MA in non-transformed cells and stimulated caspase-independent autophagic cell death in cancer cells, accompanied with mitochondrial dysfunction. Cell death induced by 2-ME was reversed by overexpressing mitochondrial SOD2, suggesting that 2-ME acts mainly as a complex I poison generating superoxide from mitochondria, and was reduced by the knockdown of Atg5 or Beclin-1 [9]. In our model, PDT-induced MA involves primarily $^{1}O_2$ photogenerated at the ER [23] and its cytoprotective action appears to be mainly Atg5 dependent, because silencing Beclin-1 does not significantly affect photokilling (M. Dewaele unpublished

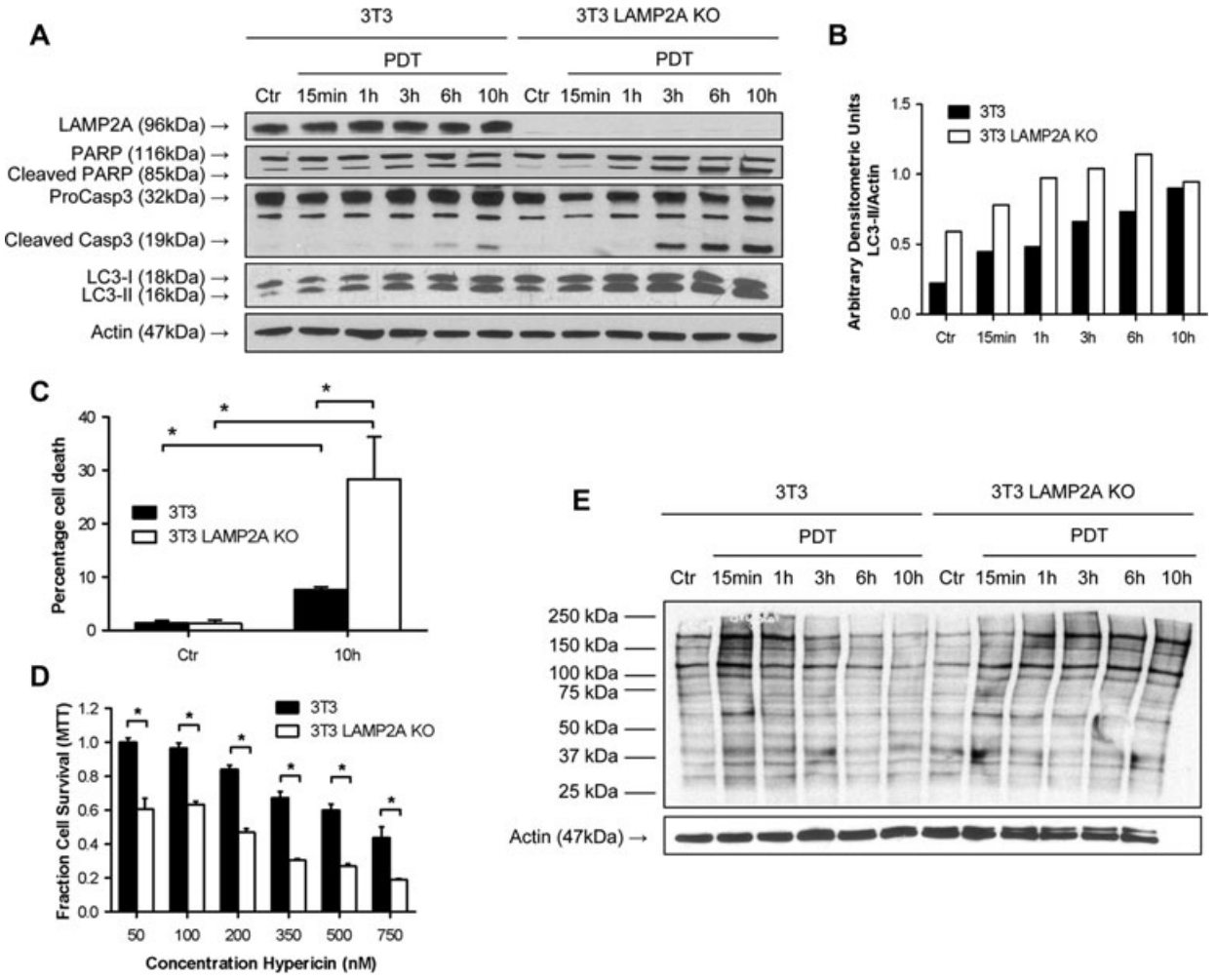

Fig. 7 CMA is involved in the survival response to oxidative stress after PDT. All controls represent incubation with hypericin without irradiation unless stated otherwise. (**A**) Whole cell lysates of 3T3 and 3T3 LAMP2A KO fibroblasts were harvested at the indicated time-points and analysed for LAMP2A, caspase 3 activation, PARP cleavage and LC3-conversion. Actin was used as a loading control. (**B**) Densitometric quantification of LC3 in the corresponding Western blot analysis in (**A**). Arbitrary densitometric units represent LC3-II levels relative to actin levels. (**C**) Effect of CMA deficiency on PDT-induced cell death. Percentage of trypan blue positive cells (dead cells) as function of time after PDT in LAMP2A WT and KO 3T3 fibroblasts. The graph represents the mean ± S.D. of two independent experiments performed in duplicate. $^*P < 0.05$ under the Student's t-test. (**D**) Representative dose–response curve for PDT treatment with different concentrations of hypericin (as indicated) in 3T3 and 3T3 LAMP2A KO fibroblasts as evaluated by MTT assay. The curve shows the surviving fraction of cells 16 hrs after treatment. Cell survival is expressed as the fraction surviving cells with respect to the controls. $^*P < 0.05$ under the Student's t-test for a 6-fold replicate. (**E**) Total cell lysates were analysed for the presence of carbonylated protein side chains after PDT in WT and LAMP2A KO 3T3 fibroblasts as described in Figure 3. During OxyBlot procedure, hypericin was omitted from the controls to minimize effects of background irradiation during manipulation of the samples.

observations). Thus, it is tempting to assume that the subcellular site of ROS production, the type of ROS and the modified targets, are crucial factors orchestrating the pro-death or pro-survival functions of MA.

Our findings indicate that along with increased apoptosis, attenuation of MA by 3-MA or Atg5 knockdown enhances the accumulation of ROS-damaged proteins in the photosensitized cells. This strongly suggests that MA participates in the removal of ROS damaged cytoplasmic components and by doing so limits PDT-mediated injury. Remarkably, Atg5 deficiency limited apoptosis and improved clearance of ROS-damaged proteins and this irrespective of a similar ROS-dependent down-regulation of Akt-mTOR pathway in both MA-competent and MA-incompetent cells. Recent data demonstrated that genetic blockage of either one of the main autophagy pathways may cause the constitutive up-regulation of the other degradation process [40, 42]. In line with this, we found that the cytoprotective effect of genetic loss of MA against PDT-mediated cell death could be attributed to the

compensatory up-regulation of CMA in unstressed Atg5$^{-/-}$ cells. Thus, the direct cross-talk between autophagy pathways likely explains why in our ROS paradigm the functional effects on cell death caused by reduction of MA or its genetic loss are radically different.

Intriguingly, LAMP2A$^{-/-}$ cells were extremely sensitized to PDT while they were protected against the ER stress agent TG. Because MA up-regulation is induced by CMA deficiency [42] these results further underscore that MA stimulation *per se*, although cytoprotective, cannot compensate for the loss of CMA in cells responding to PDT, thus suggesting that CMA is the predominant survival process activated after PDT. However, the observation that the vulnerability of LAMP2$^{-/-}$ cells to PDT is further aggravated by the addition of 3MA (Dewaele M, unpublished results), supports the concept that CMA and MA do not have overlapping cytoprotective functions.

Remarkably, increased MA ability in LAMP2A$^{-/-}$ cells is sufficient to limit ER stress-mediated cell death, in line with the reported pro-survival role of MA under most conditions linked to ER stress [15, 46]. Thus it seems that ROS damage at the ER propagates oxidative damage to other essential organelles and soluble proteins, which necessitate for their removal different degradation mechanisms establishing a unique cross-talk with cell death machinery.

The reason for the preponderant protective function of CMA in our paradigm of ROS-mediated cell death is not completely clear. It has been suggested that increased CMA activity under condition of oxidative stress may perhaps involve oxidation-mediated generation of KFERQ-like motifs in proteins that do not originally contain this sequence, thus potentially creating novel accessible substrates for CMA [16]. Oxidative stress has been shown to increase the degradation of oxidized proteins by the lysosomal proteases, their binding to LAMP2A and LAMP2A-mediated transport across the lysosomal membrane, through a mechanism requiring the transcriptional up-regulation of LAMP2A [16].

However, this still does not explain why a presumed non-selective process like MA is less potent than a highly selective process like CMA. One possible explanation could be that the type of ROS damaged cytoplasmic components, *i.e.* soluble oxidatively damaged proteins *versus* damaged organelle and insoluble aggregates, rather than their abundance, is a determinant factor. Recent studies underlying the role of protein aggregates in neurodegenerative conditions like Huntington's disease indicate that soluble proteins display higher cytotoxicity over the aggregated complexes of that same protein [47]. Therefore it is plausible that functionally aberrant substrates of CMA may more severely perturb cell viability than the insoluble cytoplasmic components cleared by MA.

Nevertheless, while clearance of oxidatively damaged proteins *per se* is a mechanism limiting the propagation of ROS injury, it is not sufficient to impede apoptosis signalling and fully sustain cellular survival, for which likely *de novo* synthesis of the degraded ROS-damaged proteins is required. This is supported by the observation that in our system apoptotic signalling proceeds at later time-points, even when the amount of oxidized proteins returns near to control levels.

Irrespective of the exact molecular mechanism underlying the unique effects of PDT on autophagy pathways, the present study suggests that interfering with these catabolic mechanisms may improve therapeutic outcome in PDT, at least in cancer cells disposing of an intact apoptotic machinery [23, 48]. Further research on the mechanisms underlying CMA activation by ROS, will be crucial to provide additional and likely more efficient targets for therapeutic intervention in PDT and possibly in other ROS-based anticancer therapies.

Acknowledgements

This work is supported by OT/06/49 grant of the K. U. Leuven and by F.W.O grants G.0492.05 and G.0661.09 to P.A. This paper presents research results of the IAP6/18, funded by the Interuniversity Attraction Poles Programme, initiated by the Belgian State, Science Policy Office. M.D.'s research is funded by a Ph.D. grant of the Institute for the Promotion of Innovation through Science and Technology in Flanders (IWT-Vlaanderen). W.M. is a postdoctoral fellow of the Fund for Scientific Research-Flanders. N.R. is a postdoctoral fellow supported by F.R.S.-FNRS (grant F/5/4/5-MCF/KP). We thank Dr. A. M. Cuervo for the LAMP2A WT and KO fibroblasts, Dr. N. Mizushima for the MEF conditionally expressing Atg5, Dr. G. Velasco for the Ras^{V12} transformed MEFs, Dr. J. Grooten for the HeLa Neo and GPx4, Dr. J. Debnath for the pBABE-GFP-LC3 vector and Dr. A. Rosenzweig for the pLNCX-Myr-HA-Akt vector. We also thank Dr. Esther Buytaert and Dr. Silvia Kocanova for help with the myrAkt overexpression, and Kristine Rillaerts and Sofie Van Kelst for excellent technical support.

Conflict of interest

The authors confirm that there are no conflicts of interest.

Supporting Information

Additional Supporting Information may be found in the online version of this article:

Fig. S1 Effect of PDT on the phosphorylation status of Akt. MEFs (top) and HeLa cells (bottom) overexpressing an HA-tagged constitutively active, myristylated Akt (MyrAkt) or the empty vector (EmpVec) were PDT treated and checked for their activational status of Akt. Due to the abundance of phosphorylated Akt in the MyrAkt-overexpressing MEFs endogenous phospho-Akt in MEFs remains undetected on Western blot. Controls were hypericin incubated but not irradiated.

Fig. S2 Parental (*i.e.* HeLa Neo) and GPx4 overexpressing HeLa cells were analysed for caspase 3 processing, PARP cleavage and LC3-conversion on Western blot as a function of time after PDT. Actin served as a loading control. Controls were hypericin-incubated but not irradiated.

Fig. S3 (**A**) Autophagy inhibition with 5 mM 3MA (left), Atg5 siRNA (middle) and Atg5 deficiency (right) on PDT-induced cell death. Percentage of trypan blue positive cells (dead cells) as function of time after PDT. The left and middle graphs represent the mean ± S.D. of two independent experiments. For the middle panel, controls represent 16 hrs incubation with the inhibitor or vehicle without irradiation. The left graph represents the mean ± S.D. of four independent experiments and one in duplicate. (*) indicates $P < 0.05$ under the Student's t-test. (**B**) MEF and Atg5$^{-/-}$ MEF were subjected to starvation in HBSS medium or to 2.2 μg/ml tunicamycin and analysed for LC3-lipidation. (**B**) *Left:* Imaging of GFP-LC3 expressing cells; controls MEF (a) and Atg5$^{-/-}$ MEF (c), PDT-treated (6 hrs) MEF (b) and Atg5$^{-/-}$ MEF (d). (**C**) Quantification of GFP-puncta. A subset of cells were analysed for their punctuated pattern. Cells were digitally processed with the ImageJ software and manually overviewed. Controls were hypericin incubated but not irradiated.

Fig. S4 (**A**) RasV12 transformed Atg5 WT and Atg5 KO MEFs were PDT treated and total protein lysates were made at the indicated time-points. Western blot indicates Atg5-Atg12 complex, cleaved/active caspase 3 and LC3-conversion. (**B**) Evaluation of nuclear fragmentation in RasV12 transformed Atg5 WT and Atg5 KO MEFs in control cells and 16 hrs after PDT with the Cell Death Detection ELISAplus. Controls were hypericin incubated but not irradiated. (**C**) Effect of PDT on chymotrypsin-like proteasome activity in MEF and Atg5$^{-/-}$ MEF. Cells were left either untreated or PDT treated. At the indicated time-points Suc-Leu-Leu-Val-Tyr-AMC protease activity (*i.e.* fluorescent units/min.) was measured. The graph represents the mean ± S.D. of two independent experiments. Controls were incubated with hypericin but not irradiated.

Fig. S5 *Top:* Representative Western blot analysis of 3T3 and 3T3 LAMP2A KO (**A**) or MEF and Atg5$^{-/-}$ MEF (**B**) for caspase 3 activation, LC3-conversion and OxyBlot at the indicated time-points after treatment with 2 μM TG. Actin was used a loading control. *Bottom:* Percentage of trypan blue positive cells (dead cells) is shown as a function of time after TG treatment (2 μM). The graph represents the mean ± S.D. of two independent experiments performed in duplicate (*) indicates $P < 0.05$ under the Student's t-test.

References

1. **Benz CC, Yau C**. Ageing, oxidative stress and cancer: paradigms in parallax. *Nat Rev Cancer*. 2008; 8: 875–9.
2. **Scherz-Shouval R, Shvets E, Fass E, *et al.*** Reactive oxygen species are essential for autophagy and specifically regulate the activity of Atg4. *EMBO J*. 2007; 26: 1749–60.
3. **Azad MB, Chen Y, Gibson SB**. Regulation of autophagy by reactive oxygen species (ROS): implications for cancer progression and treatment. *Antioxid Redox Signal*. 2009; 11: 777–90.
4. **Chen Y, Azad MB, Gibson SB**. Superoxide is the major reactive oxygen species regulating autophagy. *Cell Death Differ*. 2009; 16: 1040–52.
5. **Mizushima N, Levine B, Cuervo AM, *et al.*** Autophagy fights disease through cellular self-digestion. *Nature*. 2008; 451: 1069–75.
6. **Dice JF**. Chaperone-mediated autophagy. *Autophagy*. 2007; 3: 295–9.
7. **Cuervo AM**. Chaperone-mediated autophagy: selectivity pays off. *Trends Endocrinol Metab*. 2010; 21: 142–50.
8. **Pyo JO, Nah J, Kim HJ, *et al.*** Compensatory activation of ERK1/2 in Atg5-deficient mouse embryo fibroblasts suppresses oxidative stress-induced cell death. *Autophagy*. 2008; 4: 315–21.
9. **Chen Y, Millan-Ward E, Kong J, *et al.*** Oxidative stress induces autophagic cell death independent of apoptosis in transformed and cancer cells. *Cell Death Differ*. 2008; 15: 171–82.
10. **Yu L, Wan F, Dutta S, *et al.*** Autophagic programmed cell death by selective catalase degradation. *Proc Natl Acad Sci USA*. 2006; 103: 4952–7.
11. **Kim EH, Sohn S, Kwon HJ, *et al.*** Sodium selenite induces superoxide-mediated mitochondrial damage and subsequent autophagic cell death in malignant glioma cells. *Cancer Res*. 2007; 67: 6314–24.
12. **Chen Y, Millan-Ward E, Kong J, *et al.*** Mitochondrial electron-transport-chain inhibitors of complexes I and II induce autophagic cell death mediated by reactive oxygen species. *J Cell Sci*. 2007; 120: 4155–66.
13. **Chen F, Wang CC, Kim E, *et al.*** Hyperthermia in combination with oxidative stress induces autophagic cell death in HT-29 colon cancer cells. *Cell Biol Int*. 2008; 32: 715–23.
14. **Djavaheri-Mergny M, Amelotti M, Mathieu J, *et al.*** Regulation of autophagy by NFkappaB transcription factor and reactives oxygen species. *Autophagy*. 2007; 3: 390–2.
15. **Wang Y, Singh R, Massey AC, *et al.*** Loss of macroautophagy promotes or prevents fibroblast apoptosis depending on the death stimulus. *J Biol Chem*. 2008; 283: 4766–77.
16. **Kiffin R, Christian C, Knecht E, *et al.*** Activation of chaperone-mediated autophagy during oxidative stress. *Mol Biol Cell*. 2004; 15: 4829–40.
17. **Fulda S, Gorman AM, Hori O, *et al.*** Cellular stress responses: cell survival and cell death. *Int J Cell Biol*. 2010; doi:10.1155/2010/214074.
18. **White E, DiPaola RS**. The double-edged sword of autophagy modulation in cancer. *Clin Cancer Res*. 2009; 15: 5308–16.
19. **Mathew R, Karp CM, Beaudoin B, *et al.*** Autophagy suppresses tumorigenesis through elimination of p62. *Cell*. 2009; 137: 1062–75.
20. **Dolmans DE, Fukumura D, Jain RK**. Photodynamic therapy for cancer. *Nat Rev Cancer*. 2003; 3: 380–7.
21. **Oleinick NL, Morris RL, Belichenko I**. The role of apoptosis in response to photodynamic therapy: what, where, why, and how. *Photochem Photobiol Sci*. 2002; 1: 1–21.
22. **Buytaert E, Dewaele M, Agostinis P**. Molecular effectors of multiple cell death pathways initiated by photodynamic therapy. *Biochim Biophys Acta*. 2007; 1776: 86–107.
23. **Buytaert E, Callewaert G, Hendrickx N, *et al.*** Role of endoplasmic reticulum depletion and multidomain proapoptotic BAX and BAK proteins in shaping cell

death after hypericin-mediated photodynamic therapy. *FASEB J*. 2006; 20: 756–8.
24. **Kessel D, Arroyo AS**. Apoptotic and autophagic responses to Bcl-2 inhibition and photodamage. *Photochem Photobiol Sci*. 2007; 6: 1290–5.
25. **Xue LY, Chiu SM, Azizuddin K, *et al.*** Protection by Bcl-2 against apoptotic but not autophagic cell death after photodynamic therapy. *Autophagy*. 2008; 4: 125–7.
26. **Reiners JJ Jr, Agostinis P, Berg K, *et al.*** Assessing autophagy in the context of photodynamic therapy. *Autophagy*. 2010; 6: 7–18.
27. **Buytaert E, Matroule JY, Durinck S, *et al.*** Molecular effectors and modulators of hypericin-mediated cell death in bladder cancer cells. *Oncogene*. 2008; 27: 1916–29.
28. **Verfaillie T, Salazar M, Velasco G, *et al.*** Linking ER stress to autophagy: potential implications for cancer therapy. *Int J Cell Biol*. 2010; doi:10.1155/2010/930509.
29. **Vantieghem A, Assefa Z, Vandenabeele P, *et al.*** Hypericin-induced photosensitization of HeLa cells leads to apoptosis or necrosis. Involvement of cytochrome c and procaspase-3 activation in the mechanism of apoptosis. *FEBS Lett*. 1998; 440: 19–24.
30. **Vantieghem A, Xu Y, Assefa Z, *et al.*** Phosphorylation of Bcl-2 in G2/M phase-arrested cells following photodynamic therapy with hypericin involves a CDK1-mediated signal and delays the onset of apoptosis. *J Biol Chem*. 2002; 277: 37718–31.
31. **Rossi S, Stoppani E, Martinet W, *et al.*** The cytosolic sialidase Neu2 is degraded by autophagy during myoblast atrophy. *Biochim Biophys Acta*. 2009; 1790: 817–28.
32. **Klionsky DJ, Abeliovich H, Agostinis P, *et al.*** Guidelines for the use and interpretation of assays for monitoring autophagy in higher eukaryotes. *Autophagy*. 2008; 4: 151–75.
33. **Wullschleger S, Loewith R, Hall MN**. TOR signaling in growth and metabolism. *Cell*. 2006; 124: 471–84.
34. **Magi B, Ettorre A, Liberatori S, *et al.*** Selectivity of protein carbonylation in the apoptotic response to oxidative stress associated with photodynamic therapy: a cell biochemical and proteomic investigation. *Cell Death Differ*. 2004; 11: 842–52.
35. **Assefa Z, Vantieghem A, Declercq W, *et al.*** The activation of the c-Jun N-terminal kinase and p38 mitogen-activated protein kinase signaling pathways protects HeLa cells from apoptosis following photodynamic therapy with hypericin. *J Biol Chem*. 1999; 274: 8788–96.
36. **Nystrom T**. Role of oxidative carbonylation in protein quality control and senescence. *EMBO J*. 2005; 24: 1311–7.
37. **Salazar M, Carracedo A, Salanueva IJ, *et al.*** Cannabinoid action induces autophagy-mediated cell death through stimulation of ER stress in human glioma cells. *J Clin Invest*. 2009; 119: 1359–72.
38. **Hosokawa N, Hara Y, Mizushima N**. Generation of cell lines with tetracycline-regulated autophagy and a role for autophagy in controlling cell size. *FEBS Lett*. 2007; 581: 2623–9.
39. **Yousefi S, Perozzo R, Schmid I, *et al.*** Calpain-mediated cleavage of Atg5 switches autophagy to apoptosis. *Nat Cell Biol*. 2006; 8: 1124–32.
40. **Kaushik S, Massey AC, Mizushima N, *et al.*** Constitutive activation of chaperone-mediated autophagy in cells with impaired macroautophagy. *Mol Biol Cell*. 2008; 19: 2179–92.
41. **Massey AC, Follenzi A, Kiffin R, *et al.*** Early cellular changes after blockage of chaperone-mediated autophagy. *Autophagy*. 2008; 4: 442–56.
42. **Massey AC, Kaushik S, Sovak G, *et al.*** Consequences of the selective blockage of chaperone-mediated autophagy. *Proc Natl Acad Sci USA*. 2006; 103: 5805–10.
43. **Liu L, Wise DR, Diehl JA, *et al.*** Hypoxic reactive oxygen species regulate the integrated stress response and cell survival. *J Biol Chem*. 2008; 283: 31153–62.
44. **Weyergang A, Berg K, Kaalhus O, *et al.*** Photodynamic therapy targets the mTOR signaling network *in vitro* and *in vivo*. *Mol Pharm*. 2009; 6: 255–64.
45. **Gao N, Rahmani M, Dent P, *et al.*** 2-Methoxyestradiol-induced apoptosis in human leukemia cells proceeds through a reactive oxygen species and Akt-dependent process. *Oncogene*. 2005; 24: 3797–809.
46. **Ogata M, Hino S, Saito A, *et al.*** Autophagy is activated for cell survival after endoplasmic reticulum stress. *Mol Cell Biol*. 2006; 26: 9220–31.
47. **Bjorkoy G, Lamark T, Brech A, *et al.*** p62/SQSTM1 forms protein aggregates degraded by autophagy and has a protective effect on huntingtin-induced cell death. *J Cell Biol*. 2005; 171: 603–14.
48. **Maiuri MC, Zalckvar E, Kimchi A, *et al.*** Self-eating and self-killing: crosstalk between autophagy and apoptosis. *Nat Rev Mol Cell Biol*. 2007; 8: 741–52.